Journal of Materials Chemistry B

ROYAL SOCIETY OF CHEMISTRY

PAPER

View Article Online
View Journal | View Issue

Check for updates

Cite this: J. Mater. Chem. B, 2025, 13, 8419

Multi-stimuli-responsive degradable boronic ester-crosslinked e-spun nanofiber wound dressings†

Sofia Nieves Casillas-Popova,[a] Nishadi Dilkushi Lokuge,[a] Prerna Singh,[a] Arianna Cirillo,[a] Anna Thinphang-Nga,[a] Cameron D. Skinner,[a] Dajana Vuckovic,[a] Brandon L. Findlay[ab] and Jung Kwon Oh *[a]

Received 30th March 2025,
Accepted 5th June 2025

DOI: 10.1039/d5tb00738k

rsc.li/materials-b

Owing to their high aspect ratio of length to diameter, large surface area, large pore size, and high molecular orientation, electro-spun (e-spun) nanofibrous mats have been explored as effective nanomaterials for various applications, including wound dressings and healing materials. Of particular interest are poly(vinyl alcohol) (PVA) e-spun nanofibers that are required to be crosslinked with covalent organic bonds to retain their structural integrity in wound environments. However, conventionally crosslinked PVA nanofibers present critical drawbacks, typically including the uncontrolled release of encapsulated drug molecules. Herein, we report a robust approach that centers on the integration of boronic ester (BE) chemistry into the design of PVA e-spun nanofibers crosslinked through the formation of degradable BE crosslinks. A new phenyldiboronic acid with an ethylene spacer, which is biocompatible and has a lower pK_a value, is proved to be an effective crosslinker to fabricate BE-crosslinked PVA e-spun nanofibrous materials. In response to multiple stimuli such as reactive oxygen species, alkaline pH, and glucose (common features of wounds), the fibers degrade through the cleavage of BE bonds or transesterification, confirmed by our model spectroscopic study with a small molecular boronic ester. Such wound-induced degradation ensures the controlled/enhanced release of antibiotics active against both Gram-positive and Gram-negative bacteria. These results, combined with their non-hemolysis and non-cytotoxicity properties, demonstrate that the approach is versatile for the fabrication of well-defined BE-crosslinked PVA e-spun nanofibers that are dimensionally stable but degrade to release antibiotics in wounds, thus exhibiting a great promise as smart wound dressing materials.

Introduction

Electro-spun (e-spun) nanofibers and their fibrous mats fabricated by an e-spinning process for polymeric solutions possess a high aspect ratio of length to diameter, large surface area, large pore size, and high molecular orientation.[1–3] Because of these features, e-spun nanofibrous mats have been extensively explored as effective nanomaterials for various applications in diverse fields, including energy storage and environmental engineering,[4] as well as biosensing, drug delivery,[5–8] and particularly dressings of chronic wounds.[9–12] A variety of synthetic and naturally-occurring polymers have been e-spun into well-defined nanofibrous mats.[13] Among them, poly(vinyl alcohol) (PVA) is water-soluble (hydrophilic) and has pendant hydroxyl groups that can be used for further modification to create value-added materials. PVA possesses remarkable electrospinnability, excellent thermal and chemical stability, high water absorbing capacity, and good biocompatibility.[14–16] Moreover, e-spun PVA nanofibrous mats enable the encapsulation of hydrophilic antibacterial drugs to inhibit the proliferation of bacteria in wounds, thus promoting wound healing.

However, e-spun PVA mats need to be crosslinked because of their high solubility in water. Chemical crosslinking through the formation of covalent crosslinks is the most robust approach to retaining PVA mats with not only structural integrity in aqueous environments but also high mechanical strength and solvent resistance.[17–20] Ester,[21–23] carbamate,[24] and acetal bonds[25–28] are typical covalent crosslinks that are formed through facile coupling reactions of reactive crosslinkers with the OH pendants of PVA.

[a] Department of Chemistry and Biochemistry, Concordia University, Montreal, Quebec, H4B 1R6, Canada. E-mail: john.oh@concordia.ca
[b] Department of Biology, Concordia University, Montreal, Quebec, H4B 1R6, Canada

† Electronic supplementary information (ESI) available. See DOI: https://doi.org/10.1039/d5tb00738k

Regardless of these advances, the chemical crosslinking approach presents several drawbacks, such as harsh crosslinking conditions, concerns about the toxicity of crosslinkers, or more importantly, uncontrolled release of encapsulated antibiotics from PVA nanofibrous mats.[29–31] To achieve on-demand or controlled drug delivery, stimuli-responsive degradation (SRD) has been integrated in the design of e-spun nanofibers.[32–34] However, most reports describe SRD involving changes in hydrophobic/hydrophilic balance (*e.g.*, polarity) in response to temperature, pH, light, and electric field. SRD through chemical transition with the cleavage of labile bonds is rarely reported.

Boronic ester (BE) bonds are formed by a facile condensation reaction of boronic acid with diol, eliminating water as a side product under mild conditions (*e.g.*, room temperature with no acids or catalysts).[35–39] BE bonds have been known to be degradable (cleavable) in response to endogenous stimuli, such as alkaline pH, hydrogen peroxide, and glucose, all features of chronic and infected wounds.[40–44] Regardless of such promising stimuli-responsive degradation properties, the incorporation of BE chemistry has been limited to developing e-spun PVA nanofibrous mats, while it has been explored significantly in the design of PVA-based hydrogels.[45–49] Recently, we have demonstrated that the new approach exploring degradable BE chemistry, with a choice of a commercially available 1,4-benzene diboronic acid, enables the fabrication of well-defined, BE-crosslinked, e-spun PVA nanofibers for smart wound dressings. BE-crosslinked mats degraded through the cleavage of BE crosslinks to the corresponding boronic acids and diols in response to both acidic and alkaline pH. Such pH-responsive degradation ensured the controlled release of encapsulated levofloxacin and thus promoted their antibacterial activities against both Gram-positive and Gram-negative bacteria.[50]

Furthermore, reports describe the dependence of the substituents on the acidity of arylboronic acids *via* their inductive effects. Electron-withdrawing groups on the phenyl ring tend to increase the acidity of boronic acid, whereas electron-donating groups tend to decrease the acidity.[51,52] Furthermore, the spacers between both phenyl groups in aryl diboronic acid crosslinkers could be expected to influence their efficiency of crosslinking and eventually the properties of BE-crosslinked nanofibers. Given our preliminary proof-of-concept investigation, we have further explored the values of our approach, exploring BE chemistry to develop more robust and distinct e-spun PVA nanofibers crosslinked with degradable BE bonds to enhance wound healing.

In this work, we synthesized a new phenyldiboronic acid crosslinker with an ethylene spacer between two aryl groups (called DBA-E) through a facile coupling reaction. Because of its great acidity, low cytotoxicity, and flexibility, the synthesized DBA-E was examined as an effective diboronic acid crosslinker to fabricate e-spun PVA nanofibers crosslinked with degradable BE linkages (called BE-PVA mats). Upon our comprehensive studies of BE-induced crosslinking, stimuli-responsive degradation to pH, hydrogen peroxide, and glucose was systematically investigated for a pinacol-conjugated DBA-E (called DBA-EP) model compound by ^{1}H NMR spectroscopy and BE-PVA mats by gravimetric and microscopic analysis. Mats loaded with levofloxacin (called BE-PVA/LF) were then evaluated for not only stimuli-responsive release of encapsulated levofloxacin but also antibacterial activity against both Gram-negative and Gram-positive bacteria as well as *in vitro* hemolysis with blood and cytotoxicity with skin cell lines, demonstrating effective wound dressing materials with controlled/enhanced drug release in wound environments (Fig. 1).

Experimental

Instrumentation

^{1}H NMR spectra were recorded on a 500 MHz Varian spectrometer. DMSO-d_6 quintet at 2.5 ppm was selected as the reference standard. High resolution mass (HRMS) spectra were recorded on a Thermo LTQ Orbitrap Velos mass spectrometer equipped with a heated electrospray ion source to analyze the exact mass of compounds. A full MS spectrum (m/z 150–600) was acquired in the Orbitrap in positive mode at a resolution of 100 000. FT-IR spectra were collected by a Thermo Scientific Nicolet iS5 spectrometer equipped with an iD5 attenuated total-reflection (ATR) accessory. UV/vis spectra were recorded on a Cary 60 UV-vis Agilent spectrophotometer using a rectangular quartz cuvette with an optical path length of 1 cm.

Differential scanning calorimetry (DSC) measurements were performed using a DSC Q20 Instrument with nitrogen flow (50 mL min^{-1}). For analysis, the samples were hermetically enclosed in an aluminum pan and equilibrated at −80 °C. Two cycles were run for each sample, each cycle consisting of heating up to 250 °C at a rate of 10 °C min^{-1} and subsequently cooling to −80 °C at a rate of 5 °C min^{-1}.

Universal tensile measurements were conducted using a Z5 tensile machine (Hoskin Scientific) equipped with a 1 kN load cell to assess the mechanical properties of e-spun nanofibrous mats, including tensile strength, elongation, and Young's modulus. E-spun fibrous mats were cut into rectangular-shaped specimens (34 ± 2 mm × 10 ± 1 mm × 0.05 ± 0.01 mm), and they were loaded until failure with a steady strain rate of 5 mm min^{-1}.

Scanning electron microscope (SEM) images were obtained using a Phenom ProX with a resolution equivalent to, or less than, 8 nm and an acceleration voltage of 10 kV. Nanofibers were dried in a vacuum oven for 24 h, mounted on a stub using double-face carbon tape, and coated with a 5 nm thick layer of gold using a Cressington 108 Auto Sputter Coater. Their average diameters were calculated from more than 100 nanofibers using ImageJ software.

Materials

4-Carboxyphenylboronic acid (CPBA, >99%), 4-(dimethylamino)pyridine (DMAP, >99%), ethylene glycol (EG, 99.8%), *N*-(3-dimethylaminopropyl)-*N*′-ethylcarbodiimide (EDC, >97%), pinacol (98%), poly(vinyl alcohol) (PVA, $M_w \approx$ 89–98 kDa and >99% hydrolyzed), D-glucose (Glu, >99.5%), dibasic sodium

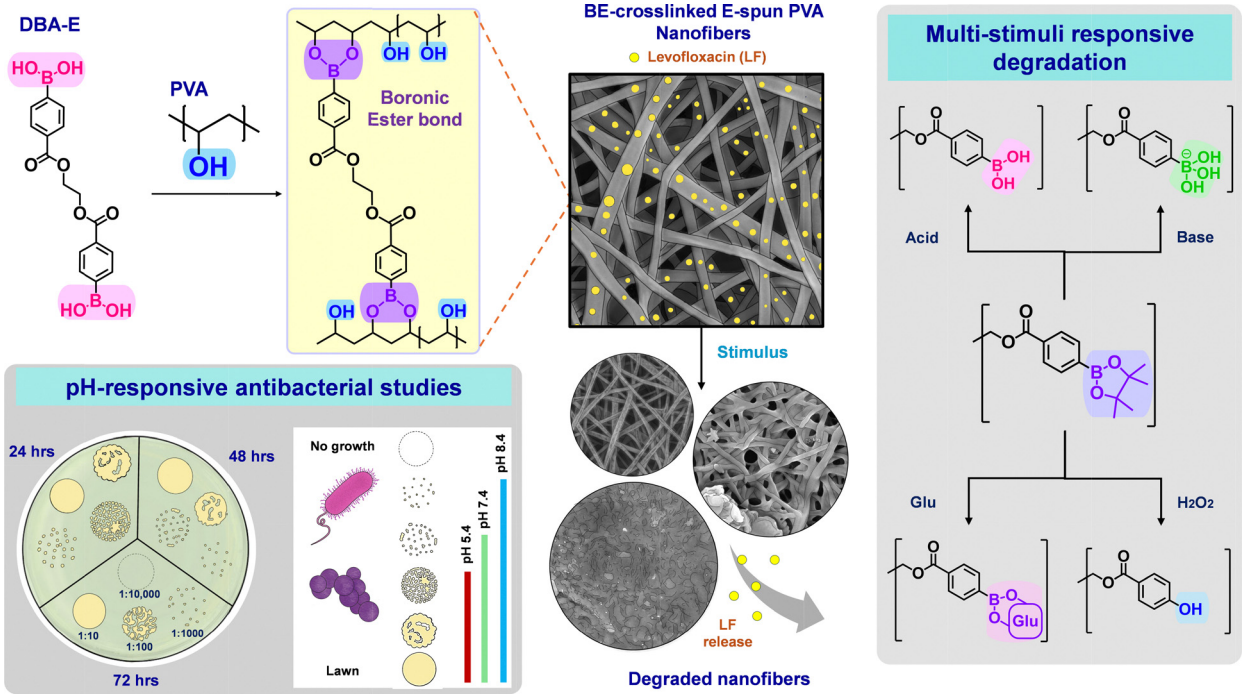

Fig. 1 Schematic illustration of our approach exploring degradable BE chemistry, with the synthesis of a new phenyldiboronic acid bearing an ethylene spacer as an effective crosslinker (DBA-E), to fabricate BE-crosslinked PVA e-spun nanofibrous mats, which exhibit the controlled and enhanced release of encapsulated antibiotics upon degradation in response to endogenous stimuli such as alkaline pH, hydrogen peroxide, and glucose, with antibacterial activity against both Gram-negative and Gram-positive bacteria.

phosphate (Na_2HPO_4, >98%), citric acid (H_3Cit, >98%), levofloxacin (LF, >98%), phosphate buffered saline (PBS) tablets, Mueller Hinton Broth 2 (MHB) microbiology culture medium, agar powder (Quality level 100), molecular sieves (pore diameter = 5 Å and bead diameter = 4–8 mesh), and aqueous hydrogen peroxide solution (H_2O_2, 9.78 M, 30%) were purchased from Millipore Sigma and used without any further purification unless otherwise mentioned. Solvents of ACS grade including *N,N*-dimethylformamide (DMF), tetrahydrofuran (THF), methanol (MeOH), and dimethyl sulfoxide (DMSO) were used as supplied. Isolated Sprague Dawley rat red blood cells (RBCs) were purchased from Fisher Scientific.

Synthesis of (((ethane-1,2-diylbis(oxy))bis(carbonyl))bis(1,4-phenylene))diboronic acid (DBA-E)

DMAP (1 mmol, 0.12 g) dissolved in DMF (1 mL) was gradually added to an organic solution containing CPBA (6 mmol, 1.0 g) and EG (2.1 mmol, 118 μL) dissolved in DMF (5 mL). EDC (6.6 mmol, 1.3 g) suspended in THF (5 mL) was then added dropwise under stirring at RT for 24 h. The resulting mixture was precipitated from cold deionized water and the precipitates were isolated by vacuum filtration. The product was collected as the third of the total of three bands of a silica gel column using MeOH as an eluent. MeOH was removed by rotary evaporation and the product was dried in a vacuum oven at 30 °C for 2 h as a white powder with a yield of 0.4 g (43%). R_f = 0.25 on silica (MeOH). ^{1}H NMR (DMSO-d_6, ppm): 8.30 (s, 4H, –B(O**H**)$_2$), 7.93 (s, 8H, Ar–**H**s), 4.63 (t, 4H, –C(O)O–C**H**$_2$–). ^{13}C NMR (DMSO-d_6, ppm): 166.00, 140.25, 134.44, 130.79, 128.18, and 62.93 ppm. Mass calculated for $C_{16}H_{16}B_2O_8H^+$: 359.1110 and found: 359.1102.

Synthesis of DBA-E pinacol ester (DBA-EP)

Purified DBA-E (0.2 mmol, 0.1 g) was mixed with pinacol (0.4 mmol, 47.3 mg) and molecular sieves in DMSO (5 mL) under stirring at RT for 24 h. The reaction mixture was subjected to centrifugation (5500 rpm, 5 min, RT) and the precipitates were washed with cold MeOH. This centrifugation-washing cycle was repeated three times. The resulting product was dried in a vacuum oven at 30 °C for 6 h to yield a white powder (60%). ^{1}H NMR (DMSO-d_6, ppm): 7.97–7.94 (d, 4H, Ar–**H**s close to ester group), 7.81–7.78 (d, 4H, Ar–**H**s close to B(OH)$_2$), 4.64 (t, 4H, –C(O)O–C**H**$_2$–), and 1.30 (s, 24H, C**H**$_3$). ^{13}C-NMR (DMSO-d_6/THF 2/5 v/v, ppm): 165.51, 137.14, 134.50, 131.86, 128.32, 84.02, 62.84, and 24.48 ppm. Mass calculated for $C_{28}H_{36}O_8B_2H^+$: 523.2669 and found: 523.2671.

UV/vis spectroscopic titration to determine the pK_a of DBA-E

A stock solution of DBA-E in MeOH was prepared by dissolving DBA-E (20 mg) in MeOH (2 mL). Its aliquot (50 μL) was diluted in 0.1 M aqueous Na_2HPO_4 solution (5 mL, pH = 9.5) to adjust the absorbance to be 0.9–1.0. Aqueous 4.5N HCl solution in microliter volume was added dropwise and the pH and UV/vis spectrum of the resulting mixtures were recorded. The pK_a of DBA-E was determined as the midpoint of the titration curve. A similar procedure was used to determine the pK_a of CPBA.

Fabrication of e-spun PVA nanofibers by e-spinning

A series of e-spun PVA nanofibers were fabricated using a home-made e-spin set-up and a syringe pump with aqueous 10 wt% PVA solution (0.5 mL). Fig. S1 (ESI†) displays the digital image of the set-up. The details of our lab-made e-spinning setup is described in our previous publication.[53]

Crosslinking of e-spun PVA nanofibers with DBA-E

The fabricated e-pun PVA nanofibrous mats ($\approx$50 mg) were immersed at RT for 48 h in DMF (15 mL) containing the various amounts of DBA-E (100, 200, 400, and 800 mg) equivalent to increasing mole equivalent ratios of BA/2OH = 0.25/1, 0.5/1, 1/1 and 2/1. The resultant mats were immersed in acetone (15 mL) for 24 h to remove DMF residues and then dried in a vacuum oven at 60 °C for 24 h. The weights of the mats before and after being crosslinked were recorded to analyze BE-crosslinked PVA mats.

Gel content measurements

Pieces ($\approx$50 mg) of BE-crosslinked PVA mats were immersed in deionized water (25 mL) for 24 h and dried for 24 h in a vacuum oven set to 60 °C. Gel content as %insoluble species in water was determined by gravimetric analysis.

Model studies of SRD with DBA-EP using ^{1}H NMR spectroscopy

For response to acidic and alkaline pH, the purified DBA-EP (7.5 mg, 14 μmol) dissolved in DMSO-d_6 (500 μL) was mixed with 1.0 M aqueous HCl solution (10 μL) and 1.0 M aqueous NaOH solution (10 μL), both of which is equivalent to $[H^+]$ or $[OH^-]$ = 0.02 M in DMSO. For response to H_2O_2, DBA-EP (5 mg, 9.6 μmol) dissolved in DMSO-d_6 (500 μL) was mixed with 9.7 M aqueous H_2O_2 solution (2 μL, equal to mole equivalent ratio of H_2O_2/BE = 1/1). For response to Glu, the purified DBA-EP (2.5 mg, 4.8 μmol) was mixed with Glu (1.7 mg, 9.6 μmol) at a mole equivalent ratio of Glu/BE = 1/1 in DMSO-d_6 (1.4 mL) in the absence and presence of NaOH. ^{1}H NMR spectra of the mixtures were recorded for given time intervals.

Stimuli-responsive degradation of BE-PVA fibrous mats

Pieces of dried BE-PVA mats ($\approx$50 mg, BA/2OH = 2/1) were prepared. To determine the pH response, pieces were immersed in buffer solutions (25 mL) at pH = 5.4, 7.4, and 8.4. McIlvaine buffer, also known as citrate–phosphate buffer, was used for this study due to its broad buffer capacity. Buffer solutions were prepared by mixing the corresponding volumes of 0.1 M H_3Cit and 0.2 M Na_2HPO_4. The degraded mats were immersed for 15 min in deionized water (50 mL) to remove any salts. For H_2O_2 response detection, the mats were immersed in 1 mM aqueous H_2O_2 solution (50 mL). For glucose response detection, mats were immersed in aqueous 126 mg dL^{-1} glucose solutions (25 mL) with and without NaOH. %Degradation was determined by gravimetric analysis.

Fabrication of LF-loaded BE-PVA nanofibrous mats

A similar procedure for electrospinning and crosslinking (BA/2OH = 2/1) as described above was applied with 10% w/w aqueous PVA solution (0.5 mL) containing various amounts of LF as 10, 20, and 25 wt%. The fabricated LF-loaded BE-PVA nanofibers were isolated and dried in a vacuum oven to remove residual DMF.

Stimuli-responsive release of LF from LF-loaded BE-PVA mats

Pieces of LF-BE-PVA mats ($\approx$25 mg) were immersed in various solutions (25 mL) at 37 °C under stirring. McIlvaine solutions at pH = 5.4, 7.4, and 8.4 were used for pH response, whereas 126 mg dL^{-1} aqueous glucose solutions with and without NaOH were used for glucose response. Aliquots (1 mL) were taken at given times to record their UV/vis spectra. Fresh buffer solution (1 mL) was added to maintain sink conditions.

To construct correlation curves of LF, a series of aqueous LF solution at 0.5–25 μg mL^{-1} was prepared by diluting an aqueous LF stock solution (100 μg mL^{-1}) with McIlvaine buffer solution (pH = 5.4, 7.4 or 8.4) for pH-responsive release. A similar procedure was used with 126 mg dL^{-1} aqueous Glu solution (pH = 7.4 and 8.4). Their UV-vis spectra were recorded.

Antibacterial studies through a Kirby-Bauer disk diffusion method

The pH values of MHB broth were adjusted to 5.4, 7.4 and 8.4 using 1 M HCl or 2 M NaOH solution. The resulting MHB agar plates were seeded with *E. coli* (ATCC 25922), *S. aureus* (ATCC 29213), and methicillin-resistant *S. aureus* (MRSA) (CANWARD 113379) from an inoculum with a density of 0.5 McFarland Turbidity Standard (equivalent to 1–2 $\times$ 10^8 colony forming units (CFU) per mL).[54] The inoculum was prepared by suspending isolated colonies in MHB media at the corresponding pH. Then, disk-shaped BE-PVA fibrous mats loaded with various amounts of LF (10, 20, and 25 wt% based on PVA) with a diameter of 8 mm ($\approx$0.5 mg) were placed onto the inoculated agar surface within 15 min after inoculation and then incubated at 35 $\pm$ 2 °C for 18 h.

A similar procedure was performed for control groups, including the BE-PVA mat (not LF loaded), LF-loaded uncrosslinked PVA mat, and filter paper with and without LF for positive and negative controls, respectively.

Broth microdilution method to determine minimum inhibitory concentration (MIC)

To establish MIC values of LF against *E. coli* (ATCC 25922) and *S. aureus* (ATCC 29213), a stock solution of LF was serially diluted in MHB culture medium to achieve a two-fold concentration range from 128 mg L^{-1} to 0.25 mg L^{-1}. A bacterial suspension was adjusted to 0.5 McFarland standard ($\sim$1–2 $\times$ 10^8 CFU per mL) and further diluted to obtain a final inoculum of $\sim 10^6$ in each well. The wells were loaded with equal volumes of diluted LF and final inoculum. The 96-well titer plate was incubated at 35 $\pm$ 2 °C for 18–20 h after which bacterial growth was assessed visually. The MIC value was recorded as the lowest concentration at which no growth was observed.

pH-responsive antibacterial suspension assay

Pieces of BE-PVA mats ($\approx$0.5 mg and 8 mm diameter) with and without LF (0.005 wt%) were sterilized under UV light on both

sides for 15 min. Inocula of *E. coli* ATCC 25922 and *S. aureus* ATCC 29213 were prepared at a working cell density of $\approx 10^6$ CFU per mL using 0.5 McFarland standard in MHB media at pH = 5.4, 7.4, and 8.4. The bacterial inocula (200 μL) were incubated with the sterilized mats in 96-well plates at 35 ± 2 °C. An aliquot (100 μL) of the bacterial suspension was collected and serially diluted at ratios of 1/10, 1/100, 1/1000 and 1/10 000 for specified time intervals of 24, 48 and 72 h. Using the spot on lawn plating technique, aliquots of the diluted suspensions (10 μL) were dispensed onto MHB agar plates of appropriate pH values and incubated for 24 h at 35 ± 2 °C. The three groups tested include bacteria with BE-PVA mats with and without LF as well as bacteria alone.

Cell viability by resazurin reduction assay

Human foreskin fibroblast cell line-1 (HFF-1) (ATCC, SCRC-1041) and Human Embryonic Kidney 293 (HEK293) (ATCC, CRL-1573) cells were cultured at 1×10^4 cell per mL per well in a 96-well plate in 100 μL of Dulbecco's modified Eagle's medium (DMEM) supplemented with 10% fetal bovine serum and 1% antibiotics (50 U mL^{-1} penicillin and 50 U mL^{-1} streptomycin) at 37 °C, 5% CO_2, and 90–95% humidity.[55] After 48 h, the culture medium was replaced and the cells were then co-cultured with sterile disk-shaped (≈0.5 mg and 8 mm diameter) BE-PVA fibrous mats loaded with and without 0.005% LF for 24, 48, and 72 h. After the given incubation times, the mats were removed and the culture media were replaced with fresh DMEM media with 10% resazurin solution (0.15 mg mL^{-1}, 10 μL). The resazurin solution was sterilized prior to use by filtration through a poly(ethene sulfone) membrane with a 0.2 μm pore size. A PerkinElmer EnSight plate reader was used to record the absorbances of the culture media at λ = 570 and 600 nm following a 3 h incubation period.[56]

Cell viability for DBA-E alone with HEK293 cells was evaluated after a 24-hour exposure period using the same protocol as for the nanofiber mats. A final concentration of 5–10 μM of DBA-E in the wells was achieved by diluting a sterile stock solution of DBA-E in DMSO (0.5 mg mL^{-1}) with DMEM culture medium. The previous cell culture media was replaced with fresh culture medium containing DBA-E at the time of treatment application.

In vitro hemocompatibility assay

Sprague Dawley rat RBCs were used to evaluate the hemocompatibility for BE/PVA nanofibers with and without LF (0.005%). RBCs as received were diluted in sterile PBS solution (2 wt% RBC suspension) and subjected to centrifugation (1000*g* × 5 min × 4 °C) to obtain transparent, pink-colored supernatant (indicating that RBCs were not hemolyzed and were ready for tests). Sterilized disk-shaped BE/PVA nanofibers (≈0.5 mg, 0.8 mm in diameter, 0.05 mm in thickness) with and without LF were incubated in the RBC suspension (0.7 mL) for 4 h at 37 ± 2 °C under gentle stirring. The mats were then removed and the suspension of RBCs was subjected to centrifugation (1000*g* × 5 min × 4 °C). The absorbance of the supernatant was measured at λ = 577 nm and 620 nm as references. RBCs suspended in deionized water were used as the positive control and PBS as the negative control were included.

Results and discussion

Synthesis of DBA-E

Fig. 2a illustrates our approach to synthesizing a new DBA-E crosslinker with ethylene spacer between phenylboronic acids. This approach explores a facile EDI-mediated coupling reaction of 2 moles of CPBA with 1 mole of EG through the formation of ester bonds in a mixture of DMF/THF at room temperature, yielding DBA-E phenyldiboronic acid. Excess CPBA (1.4 mole equivalent to OH group of EG) was used to minimize the formation of a monosubstituted product, thus promoting the synthesis of DBA-E. After the removal of *N*-acyl urea byproduct, the chemical structure of the product was characterized by standard analytical techniques. The ^{1}H NMR spectrum in Fig. 2b shows a peak at 4.63 ppm (c) corresponding to methylene protons adjacent to ester bonds and a peak at 7.93–7.87 ppm (b) corresponding to phenyl protons. Their integral ratio was quantitative to the number of their protons. This result, along with ^{13}C NMR (Fig. S2, ESI†) and high-resolution mass (experimental) spectrometry, confirms the successful synthesis of DBA-E.

pK_a determination and biological activity of DBA-E

The new DBA-E consists of the BA group on a phenyl ring substituted with a carbonyl group in its *para* position. To see how the *p*-carbonyl group affects the acidity of the phenylboronic acid, the pK_a of DBA-E was determined using a spectroscopic titration method.[52,57] From the UV/vis spectra of DBA-E in the pH range of 5.5–9.5 (Fig. S3, ESI†), the titration curve with absorbance at λ = 285 nm was constructed over this pH range (Fig. 2c). The pK_a of DBA-E (with *p*-carbonylester on the phenyl ring) was determined to be 7.7 at its mid-point. This value is comparable with the pK_a of 7.8 for 4-formylphenylboronic acid (*p*-aldehyde), but smaller than that (8.9) for benzeneboronic acid (*p*-hydrogen). This is because carbonylester and aldehyde groups on the phenyl ring are electron-withdrawing groups.[51,52] Using a similar protocol with the spectroscopic titration method, the pK_a of CPBA was determined to be 8.3 (Fig. S4 and S5, ESI†), which is consistent with that (8.3) reported in the literature.[51]

Furthermore, DBA-E was examined for its biological activity using a resazurin reduction assay to measure the viability of HEK293 cells for 24 h. As shown in Fig. 2d, the viability was >80% in the presence of DBA-E, up to 9 μM, suggesting that DBA-E is not toxic to cells, thus is biocompatible.

Fabrication of BE-crosslinked e-spun PVA nanofibers

A home-made e-spinning set-up with a syringe pump was used for 10 wt% aqueous PVA solution. The optimized conditions were found with a BD needle 25 G 1 $\frac{1}{2}$ (0.15 mm inner diameter), a voltage of 25 kV, a flow rate of 0.85 mL h^{-1}, and a distance nozzle-collector of 9 cm. Our protocol allows for the fabrication

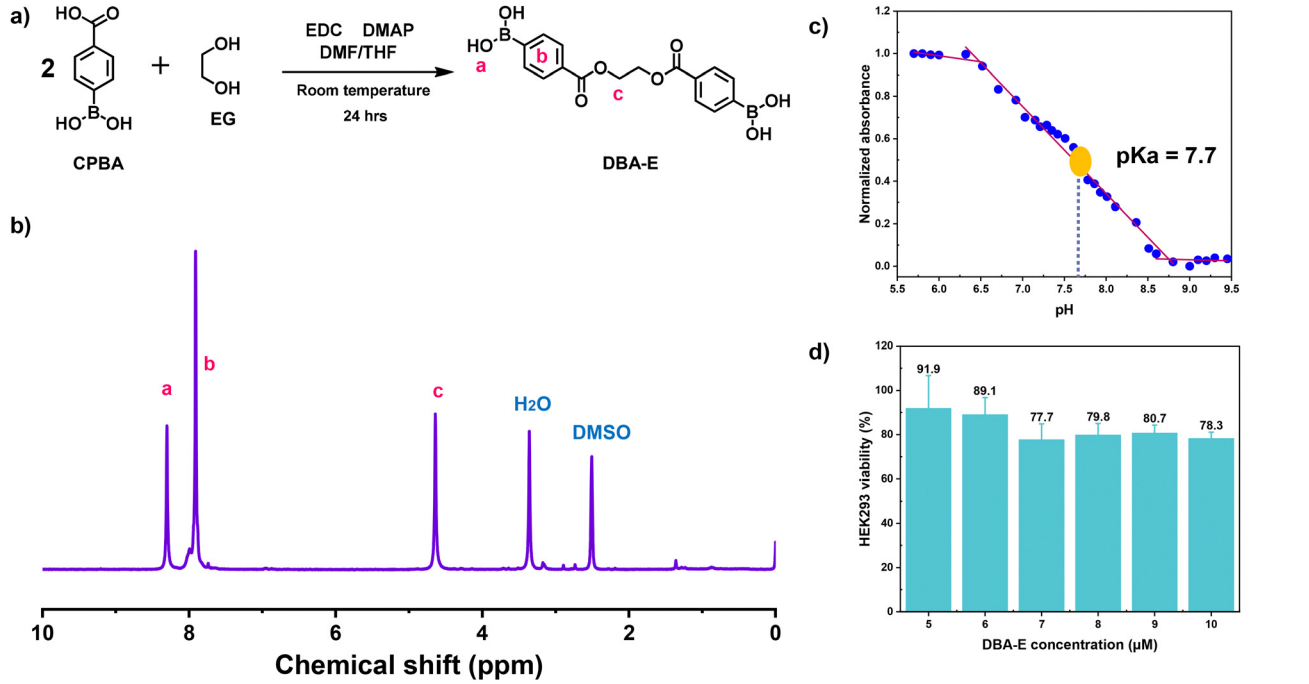

Fig. 2 For a new DBA-E phenyldiboronic acid crosslinker: synthesis exploring an EDC-mediated coupling reaction (a), ^{1}H NMR spectrum in DMSO-d_6 (b), spectroscopic titration curve of normalized absorbance at λ = 285 nm over a pH range of 5.5–9.5 (c), and viability of HEK293 cells incubated for 24 h using a resazurin reduction assay (d).

of e-spun PVA fibrous mats with well-defined, droplet-free, and randomly aligned nanofibers. The average diameter of the fibers was 139.3 ± 34.7 nm, by SEM analysis.

Because of being uncrosslinked, the fabricated PVA fibers could lose their fibrous forms and turn to jelly-like aggregates when exposed to aqueous solution. To ensure their structural integrity, PVA fibrous mats were treated with DBA-E phenyldiboronic acid crosslinker in DMF at the mole equivalent ratio of BA/2OH = 2/1 (excess of BA groups to OH groups) at room temperature. The choice of the solvent is important because our protocol to fabricate BE-crosslinked fibers utilizes the post-crosslinking approach of e-spun PVA nanofibers in an organic solvent. DMF was examined because while it is a poor solvent for PVA, enabling PVA nanofibers to retain the structural integrity, it is a good solvent for DBA-E, allowing for a high solubility of up to 109 mg mL^{-1}.

As illustrated in Fig. 3a, such crosslinking reactions allow for the fabrication of BE-crosslinked PVA fibrous mats (called BE-PVA mats) through the formation of BE crosslinks between BA groups of DBA-E and pendant hydroxyl groups of PVA chains. As shown in Fig. 3b, the crosslinked fibers appeared to be opaque (see digital image) and moreover remained intact as spaghetti-like nanofibers. They had an average diameter of 128.8 ± 35.6 nm, which is smaller than that for the corresponding uncrosslinked fibers. This kind of decrease in diameter is plausibly attributed to effective crosslinking of PVA chains in the formation of fibers in DMF.

Furthermore, to study the BE-induced crosslinking reaction, two key parameters were determined for BE-PVA mats (BA/2OH = 2/1) by gravimetry analysis. The %efficiency of DBA-E incorporated into fibers, based on the amount of DBA-E in the recipe, was determined to be 2.2%. The %hydroxyl groups in PVA fibers reacted with BA groups (*e.g.* DBA-E) to form BE crosslinks was 16%. PVA fibers could not be fully saturated (or swollen) in DMF because PVA is rarely soluble in DMF. DBA-E could have a limited capacity to diffuse inside PVA fibers. Consequently, this could restrict crosslinking through the reaction of pendant OH with a boronic acid in DBA-E to mostly the nanofiber surfaces, resulting in a low %efficiency of DBA-E incorporation and %OH reacted with DBA-E in the fibers. Promisingly, the gel content as %insoluble species of crosslinked fibers in water was 89%. These results suggest that our protocol for crosslinking PVA fibers with the use of DBA-E crosslinker appears to be effective to induce BE crosslinks in PVA fibers.

We further characterized the BE-PVA mats for their chemical structures and mechanical properties. Fig. 3c shows the B^{11} NMR spectrum of the BE-PVA mat, compared with that of DBA-E. The BE-PVA mat had two distinct peaks at 17.41 and 9.80 ppm which appear upfield, compared with those at 20.07 and 9.42 ppm for DBA-E. Such shift could be caused by changes in shielding/deshielding of the boron atoms in BA and BE forms. Given that the observed chemical shift was within the range of +50 to 0 ppm, it was determined that the boronic ester bond formed was in its three-coordinated form.[58–60] Typically, the boronic acid in the three-coordinate form is downfield shifted (0–50 ppm) in contrast to the hydroxyboronate anion (−100 to 0 ppm). Fig. 3d compares its FT-IR spectrum with those of PVA and DBA-E. It shows a strong absorption band at 1309 cm^{-1} which corresponds to the B–O stretching mode,[61–63]

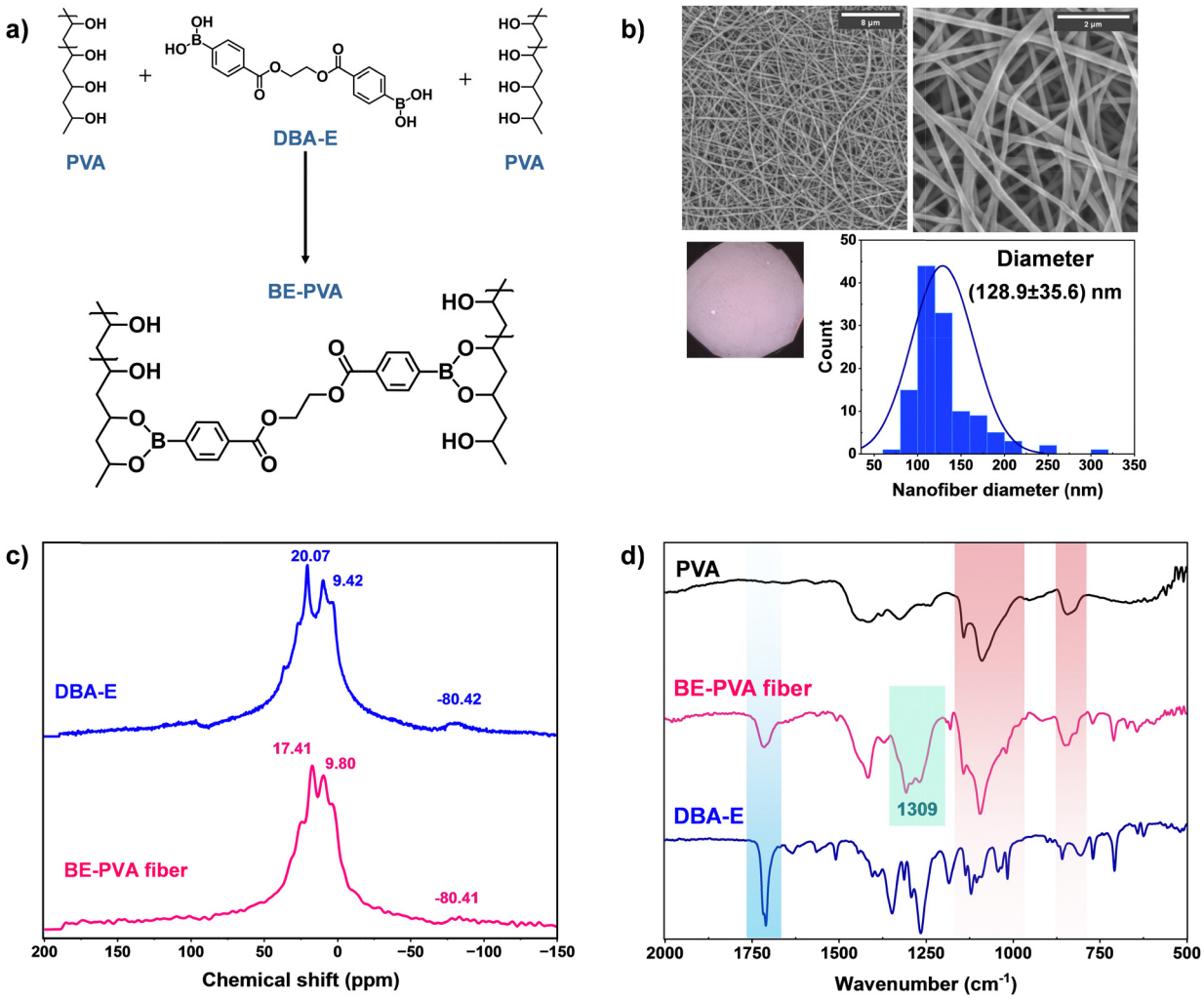

Fig. 3 Schematic illustration of BE-induced crosslinking between the pendant OH groups of PVA with BA groups of DBA-E at a mole equivalent ratio of BA/2OH = 2/1 (excess of BA groups, *e.g.* DBA-E), yielding BE-PVA mats (a); SEM images with different magnifications (scale bar = 8 μm on left image and 2 μm on right image), digital images, and size distributions of the BE-PVA mats (b); ^{11}B NMR spectrum of the BE-PVA mat, compared with that of DBA-E (c); and FT-IR spectrum of the BE-PVA mat, compared with those of PVA and DBA-E (d).

confirming the formation of new BE crosslinks. Note that the spectrum also shows a broad absorption peak at 3200–3500 cm^{-1}, characteristic of the O–H stretching vibration, confirming a large population of unreacted OH groups in PVA mats.

Fig. S6 (ESI†) shows the stress–strain curve of BE-PVA mats, compared with that of uncrosslinked mats, by universal tensile measurements and summarizes their Young's modulus, tensile strength, and elongation at break. The tensile strength and Young's modulus for the BE-PVA mats were 12.5 kPa and 5.2 kPa respectively, which were greater than those for their uncrosslinked counterparts (9.8 kPa and 4.2 kPa respectively). The elongation at break for the BE-PVA mats was 6.9%, which was lower than that (13.5%) for the uncrosslinked counterparts. These results could be attributed to the effective crosslinking of e-spun PVA fibers through boronic ester bond formation.

Overall, these results obtained from our systematic characterization using gravimetry, microscopic and spectroscopic analysis confirm that our protocol with DBA-E in DMF enables the fabrication of well-defined BE-PVA mats with spaghetti-fibers whose morphologies remained unchanged and intact during the crosslinking process.

Given our systematic studies on BE-induced crosslinking of PVA fibers with DBA-E, the effect of the amount of DBA-E as the mole equivalent ratio of BA/2OH = 0.25/1, 0.5/1, 1/1, and 2/1 was investigated. The %efficiency of DBA-E gradually increased with an increasing ratio and reached 2.5% with BA/2OH = 2/1 (Fig. 4a). The %hydroxyl group reacted with BA groups in PVA also gradually increased with an increasing ratio and reached 16% with BA/2OH = 2/1 (Fig. 4b). On the other hand, the gel content of the BE-PVA fibers in water significantly increased to 89% when the ratio increased to 1/1 and then slowly increased to 97% upon further increasing the ratio to 2/1 (Fig. 4c). These results suggest that the e-spun PVA fibers turned out to be structurally stable (*e.g.* crosslinked) even though only a small population of OH groups (<20 mol%) react with DBA-E crosslinker in DMF.

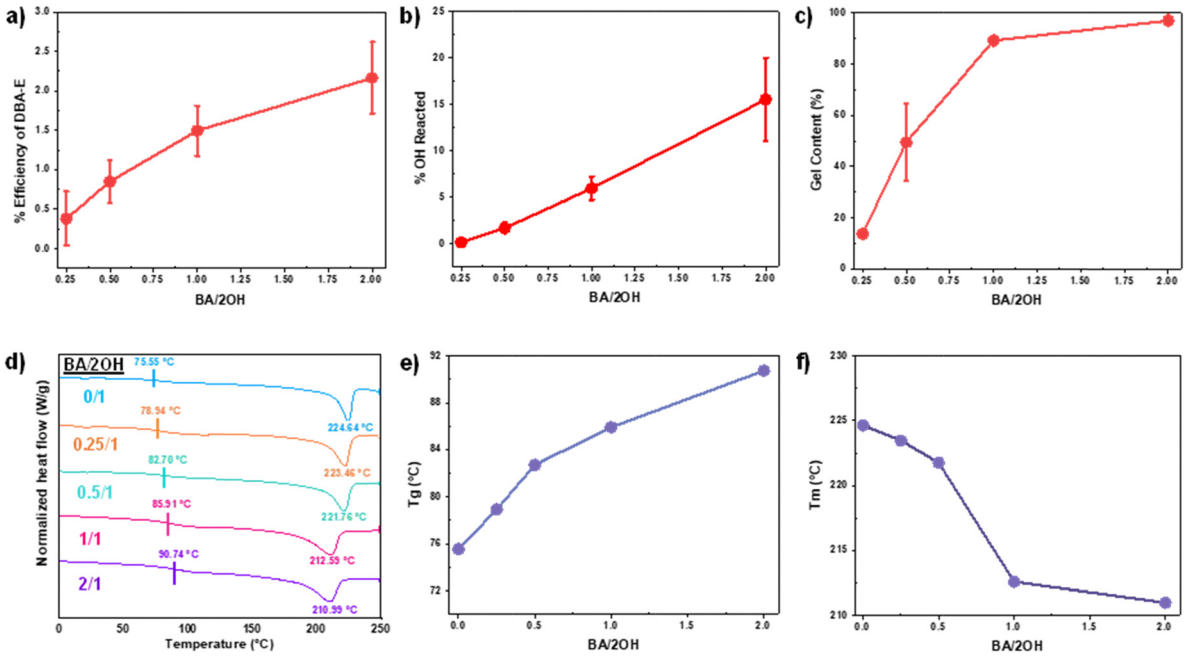

Fig. 4 Effect of the amount of DBA-E as the mole equivalent ratio of BA/2OH using gravimetry on the %efficiency of DBA-E incorporated into fibers (a), %OH reacted with DBA-E (b), and gel content as %insoluble species of BE-PVA mats in water (c); overlaid DSC thermograms (d) and thermal properties as T_g (e) and T_m (f) for BE-PVA mats fabricated with various amount of DBA-E as the mole equivalent ratio of BA/2OH.

The formed BE-PVA mats with various mole equivalent ratios of BA/2OH were characterized for their thermal properties by DSC analysis. Fig. 4d shows their overlaid DSC thermograms in a range of 0–200 °C and all thermograms exhibit a single glass transition (T_g) and melting transition (T_m). With an increasing amount of DBA-E (*e.g.* BA/2OH mole equivalent ratio), their T_g increased (Fig. 4e) while their T_m decreased (Fig. 4f). Such changes could be attributed to an increase in crosslinking density of PVA fibers.

In a separate experiment, THF was examined as a medium for the fabrication of BE-PVA mats treated with DBA-E crosslinker using a similar process in DMF. The mole equivalent ratio of BA/2OH = 1/1 was chosen, because of the limited solubility of DBA-E in THF (5.44 mg mL^{-1}). Table S1 (ESI†) compares the characteristics and properties of BE-PVA mats crosslinked with DBA-E in THF and DMF. All outputs including %efficiency of DBA-E, %OH groups reacted, and gel content were lower with THF than DMF, suggesting that crosslinking with DBA-E could be more effective in DMF than THF. Hildebrand solubility parameters reflect the structural similarity and polarity of the chemicals of interests. The greater the affinity, the closer the Hildebrand parameters are. The Hildebrand solubility parameter of PVA is 22–25 $MPa^{1/2}$, which is closer to that of DMF than THF (21.7 *vs.* 18.6 $MPa^{1/2}$ in Table S1, ESI†), meaning that PVA has a greater affinity toward DMF compared with THF. In addition to the better solubility of DBA-E in DMF over THF, the greater affinity of PVA to DMF compared with THF could attribute to better crosslinking of PVA with DBA-E in DMF than THF.

Model studies of stimuli-responsive degradation of BE bonds

To obtain better insight into the cleavage of BE bonds in response to endogenous stimuli, DBA-EP, a model phenyldiboronic ester, was synthesized through the esterification of DBA-E with pinacol at their stoichiometric balance in DMSO (Fig. S7a (ESI†) and Fig. 5a for its chemical structure). Our spectroscopic analysis including ^{1}H NMR (Fig. S7b, ESI†), ^{13}C NMR (Fig. S7c, ESI†), and HR-MS confirm the synthesis of DBA-EP through the formation of a BE bond.

Given the synthesis of DBA-EP, stimuli-responsive degradation of BE bonds was investigated using ^{1}H NMR spectroscopy. Fig. 5a illustrates the degradation of DBA-EP to its degraded products including pinacol in response to acid, base, H_2O_2, and glucose. DBA-EP was incubated with HCl (an acid) and NaOH (a base) for the pH response, in 1 mM H_2O_2 (equivalent to H_2O_2/BE = 1/1 mol equivalent ratio) for the ROS response, and in the presence of Glu with and without NaOH (equivalent to Glu/BE = 1/1 mol equivalent ratio) for the diol response. Note that the concentration of Glu was set at 126 mg dL^{-1}, which is the lowest concentration in blood for a patient diagnosed with diabetes. As seen in Fig. S8–S12 (ESI†), the overlaid ^{1}H NMR spectra show changes in peaks and their integrals over the incubation time in response to those stimuli.

For acid response, as an example, a new peak at 7.93 ppm corresponding to aromatic protons in phenylboronic acid moieties generated upon the cleavage of BE bonds appeared and its integral increased over incubation time. Two doublet peaks at 7.97–7.94 and 7.81–7.78 ppm correspond to aromatic protons in pinacol ester moieties and their integrals decreased over time. More interestingly, the integral of the peak at 1.06 ppm presenting pinacol generated upon the cleavage of BE bonds increased, while the integral of the peak at 1.30 ppm presenting pinacol ester decreased. For responses to other stimuli, similar changes in NMR peaks and their integrals, particularly pinacol

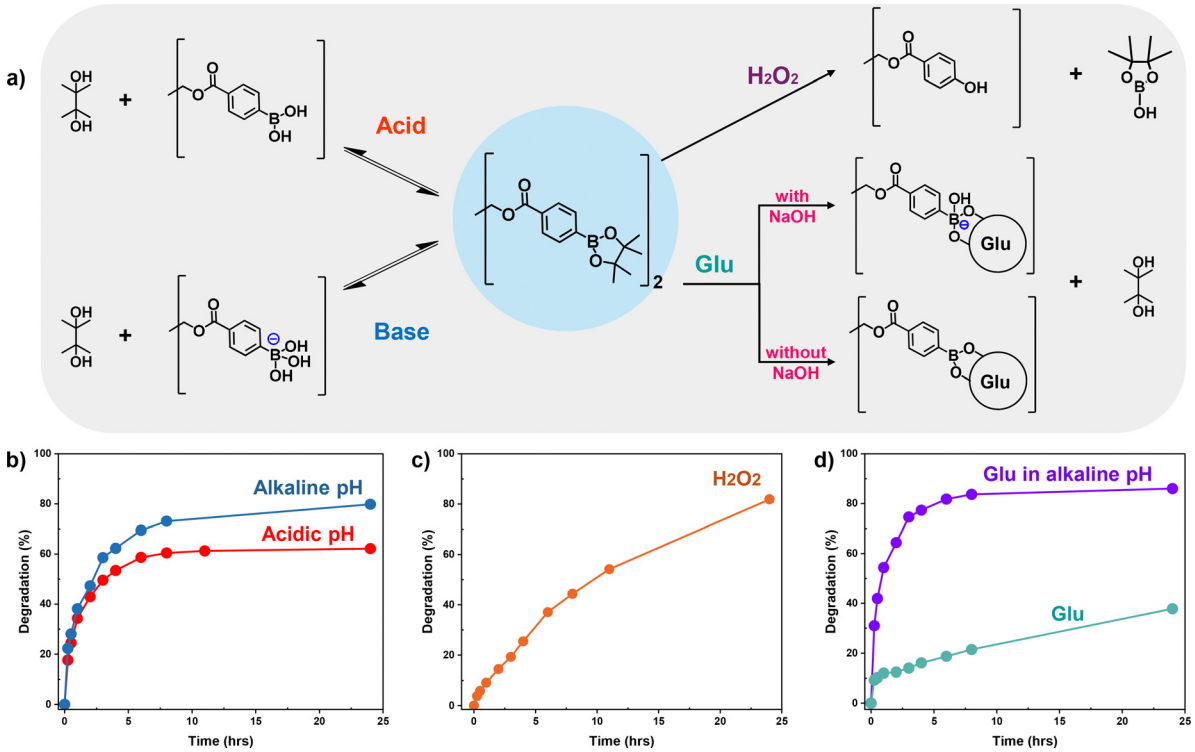

Fig. 5 Schematic illustration of DBA-EP degradation in response to HCl (acid), NaOH (base), H_2O_2, and Glu (a) and the %degradation over incubation time with HCl and NaOH (b), H_2O_2 at BE/H_2O_2 = 1/1 (c), and Glu with and without NaOH at BE/Glu = 1/1 (d).

and pinacol ester peaks, were observed. Their integral ratios allow us to calculate the %degradation of BE bonds in DBA-E.

Fig. 5b–d show our results. At acidic pH through acid-catalyzed hydrolysis of BE bonds, the %degradation increased to 62% with acid in 4 h and then gradually increased over 24 h (Fig. 5b). In the presence of NaOH, it increased to 80% in 4 h, suggesting faster cleavage of BE bonds through base-catalyzed hydrolysis, compared with acid-catalyzed hydrolysis of BE bonds (Fig. 5b). Upon exposure to H_2O_2, the %degradation rapidly increased to 88% in 25 h (Fig. 5e). Such degradation could be attributed to the cleavage of BE bonds. In the presence of Glu, it gradually increased to 38% over 25 h, which could be through the transesterification of BE bonds with Glu. In the presence of NaOH, the %degradation rapidly increased to 86% in 4 h, suggesting that the %degradation in response to Glu could be enhanced with NaOH.

Stimuli-responsive degradation of BE-PVA fibers

Given our studies on stimuli-responsive cleavage of BE bonds with DBA-EP, we investigated the degradation of BE-crosslinked PVA nanofibers in response to different pH values (acidic, neutral, and alkaline), H_2O_2, and glucose in aqueous environments. Pieces of fibrous mats were incubated in buffer solutions at different pH values = 5.4, 7.4, and 8.4, 1 mM aqueous H_2O_2 solution, and 126 mg dL^{-1} aqueous Glu solution. Their degradation was followed by %degradation as a change in masses by gravimetry analysis and changes in morphologies by SEM analysis.

When PVA mats were incubated at various pH values, the %degradation was slowly increased to 3% at all three pH values over 3 days and further increased to 6.7% at pH = 5.3, 15.9% at pH = 7.4, and 20.8% at pH = 8.4 upon an increase in incubation time up to 10 days (Fig. 6a). This result suggests that mats degraded at all tested pH values. Our SEM analysis confirms the loss of their spaghetti-like fibrous structures after being incubated at these pH values (Fig. 6d). As expected, their degradation was faster at pH 8.4 (alkaline), compared with pH 7.4 (neutral). Interestingly, the mats degraded more slowly at pH 5.3 (acidic), which does not seem to reflect the rapid acid-catalyzed hydrolysis of BE bonds to pinacol diol and corresponding DBA-E. The plausible reason could be due to gravimetry analysis based on the change in mass of mats before and after incubation, even though BE crosslinks could be cleaved in the presence of acid.

In 1 mM H_2O_2 solution, the %degradation gradually increased to 39% in 3 days and further increased to 63% in 10 days (Fig. 6b). Such degradation of fibers could be attributed to the cleavage of BE bonds as confirmed by the degradation of DBA-EP. Promisingly, their %degradation is somewhat competitive to that (89%) of small molecule DBA-EP, suggesting that H_2O_2 is an effective stimulus to the cleavage of BE bonds. Consequently, the fibers significantly lost their fibrous structures, based on SEM analysis (Fig. 6e).

Fibrous mats were immersed in aqueous Glu solutions with and without NaOH. As compared in Fig. 6c, the %degradation increased to 24%, and to 39% in the presence of NaOH in

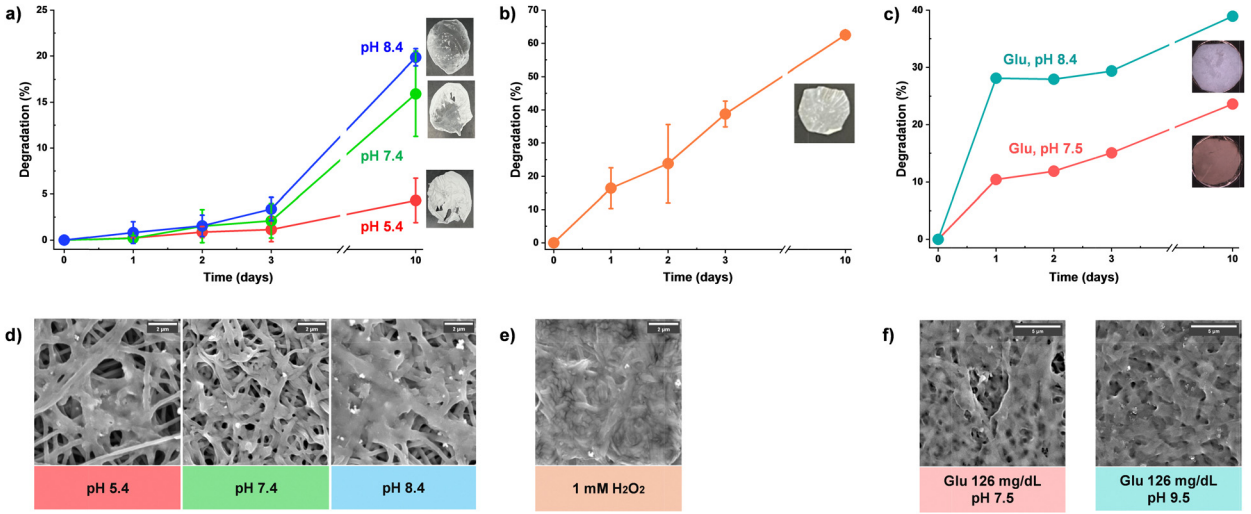

Fig. 6 %Degradation with digital images (a)–(c) and SEM images (d)–(f) of BE-PVA mats upon incubation at pH = 5.4, 7.4, and 8.4 (a) and (d), in 1 mM aqueous H_2O_2 solution (b) and (e), and in 126 mg dL^{-1} aqueous Glu solution with and without NaOH (c) and (f). Scale bars = 5 μm (d) and (f) and 2 μm (e).

10 days. A plausible reason could be due to the synergistic degradation of mats in the presence of Glu (through transesterification of pinacol ester with Glu) and at alkaline pH. Similarly, SEM analysis confirmed the loss of fibrous structures (Fig. 6f).

Given our model studies on the degradation of DBA-EP, the BE-crosslinked PVA fibers could degrade to the corresponding PVA with either DBA-E under acid or alkali pH conditions, a diphenol in hydrogen peroxide, or DBA-E/glucose in glucose. PVA is known to be non-cytotoxic and thus FDA-approved as well as reported to have no negative effect on short-term wound dressing.[64,65] DBA-E was tested to be non-cytotoxic up to 10 μM with the HEK293 cell line (see Fig. 2d). In addition, two other degraded precursors (a diphenol and DBA-E/glucose) could be anticipated to be non-cytotoxic within the concentration of DBA-E used to crosslink PVA fibers.

Loading and acid-responsive release studies

LF-loaded BE-PVA fibers (called BE-PVA/LF mats) were fabricated using our standard protocol for electrospinning with aqueous PVA solution containing LF. The amount of LF was varied at 10, 20, and 25 wt% to examine its antibacterial properties at different pH values. Fabricated BE-PVA/LF mats were analyzed for their morphologies using SEM. Typically, nanofibers fabricated at 10 wt% had an average diameter of 156.7 ± 32.4 nm, which is larger by *ca.* 30 nm, compared with that (128.8 ± 35.6 nm) for counterparts with no LF (Fig. 7a).

Furthermore, BE-PVA/LF mats were tested for their mechanical properties using universal tensile measurement to investigate if the incorporation of high doses of LF (up to 25 wt% of PVA) could affect their mechanical properties. The BE-PVA/LF (25%) mat was examined with the BE-PVA mat (no LF loaded) for comparison. As seen in their stress–strain curves in Fig. S13 (ESI†), the BE-PVA/LF mats had a tensile strength of 11.1 kPa, which was lower than that (12.5 kPa) of LE-free mats. Their elongation at break (23.4%) turned out to be greater than that (6.9%) of LF-free mats. These results suggest that LF could act as a plasticizer to make BE-PVA mats soften.

To investigate the release of LF from nanofibers by UV/vis spectroscopy, the correlation curves of LF were constructed from UV/vis spectra with different stimuli (*e.g.* pH = 5.4, 7.4, and 8.4 as well as 126 mg dL^{-1} Glu) (Fig. S14, ESI†). LF-loaded mats were incubated, and their UV-vis spectra were recorded. Given the correlation curves, the %release of LF from LF-BE-PVA mats was determined over given times. At three pH values, the %release increased in 6 h and then gradually increased up to 72 h (Fig. 7b). The %release appeared to be faster in the order of pH = 8.4 > 7.4 > 5.4, whose trend is consistent with pH-responsive degradation. In the presence of Glu, the %degradation increased in 6 h and then gradually increased up to 73 h (Fig. 7c). It was greater when NaOH was formulated, whose trend is similar to Glu-responsive degradation. The %release in response to the H_2O_2 stimulus was not examined because of possible oxidation of LF by H_2O_2 (see Fig. S15, ESI†).

Antibacterial activity and biocompatibility of the BE-PVA/LF mats

Infected skin is either neutral or alkaline (pH = 7.4 or 8.4), while healthy skin is slightly acidic (pH = 5–6). pH is known to be an important stimulus in chronic wounds and infections, significantly affecting healing rates.[66–68] To investigate the effect of pH values on antibacterial activities, BE-PVA/LF mats were first evaluated by a modified version of the Kirby-Bauer disk diffusion method at pH = 5.4, 7.4, and 8.4 against *Escherichia coli* (Gram-negative), *Staphylococcus aureus* (Gram-positive), and MRSA (Gram-positive) bacteria.[69,70] These strains of bacteria were chosen because of their significance in wound infection. In particular, *S. aureus* prevails as the most frequent cause of wound infections, accounting for around 30% of all cases, whilst *E. coli* can be found in infected wounds due to fecal contamination. MRSA is a multidrug-resistant strain of *S. aureus*.[71,72]

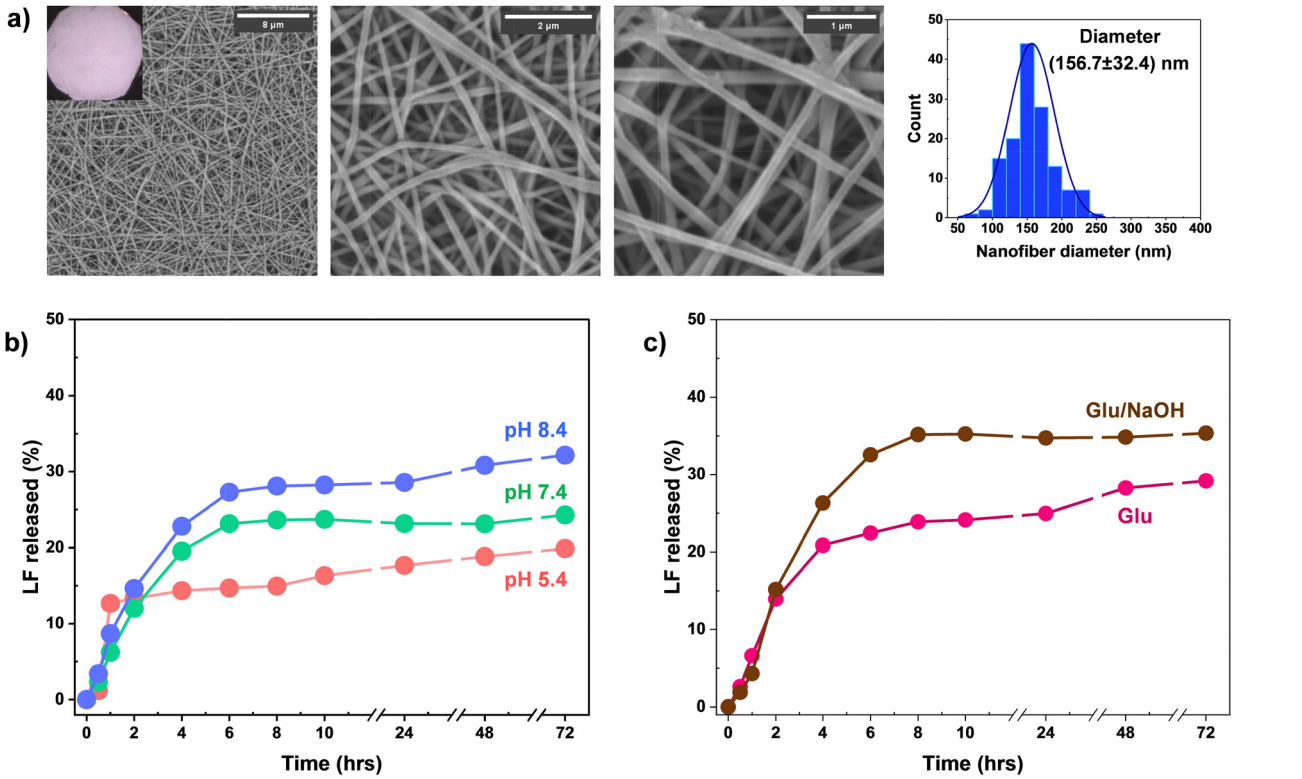

Fig. 7 SEM images with different magnifications and histogram of BE-PVA/LF mats (10 wt% loading) (a) and release profile of LF at different pH values (b) and in 126 mg dL^{-1} Glu solution with and without NaOH (c).

Following the promising result showing bacterial growth on agar plates adjusted to pH values of 5.4, 7.4, and 8.4 (Fig. S16, ESI†), disk-shaped mats were placed onto agar plates inoculated with bacterial strains at the specified pH. After incubation, the diameter of inhibition (DOI) was determined as a measure of their antibacterial activity. As shown in Fig. 8a, Gram-negative *E. coli* had a DOI of 1.5–4.5 cm at the three pH levels. The DOI increased with an increasing amount of LF in the fibers. Interestingly, the DOI increased in the order of pH = 5.4 (acidic) < 7.4 (neutral) < 8.4 (alkaline), whose order is consistent with the pH-responsive %degradation of mats and %release of LF. As seen in Fig. 8b and c, both Gram-positive *S. aureus* and MRSA had DOI values of 1.5–3 cm. The DOI increased only slightly as the amount of LF load increased. Interestingly, no significant difference in DOI was observed among the three pH values. This may be because the concentration of LF in the fibers was below the concentration required to inhibit bacterial growth.

In an experiment, controls including the BE-PVA mat without LF, uncrosslinked mat and filter paper both with and without LF were tested for their antibacterial properties against the three bacterial strains at the three pH values. Note that the same amount of LF (32 ng) was inoculated for comparison. As shown in Fig. S17 (ESI†), the BE-PVA mat and paper with no LF had a DOI of <0.2 cm, suggesting no significant antibacterial activity. On the other hand, the LF-loaded uncrosslinked mat and paper loaded with LF had a DOI greater than 4 cm, suggesting important antibacterial activity which could be

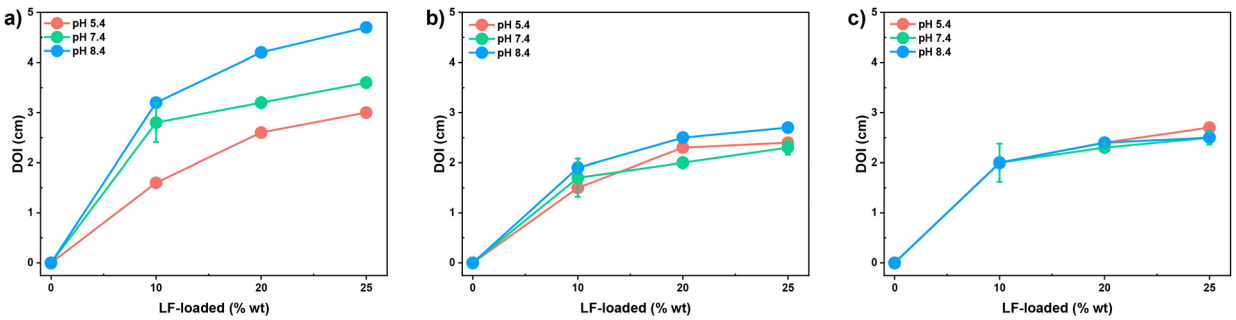

Fig. 8 The DOI of the BE-PVA mats loaded with various amounts of LF (10, 20, and 25% based on PVA) at different pH values of 5.4 (acidic), 7.4 (neutral), and 8.4 (alkaline) to evaluate antibacterial activities against *E. coli* (a), *S. aureus* (b), and MRSA (c).

attributed to the release of LF. These results confirm the validity of the modified version of our disk-diffusion method.

In another experiment, BE-crosslinked and uncrosslinked PVA mats with and without LF were placed onto agar plates at pH 7.4 containing phenol red as an indicator. As shown in Fig. S18 (ESI†), no change in color was observed after 24 h inoculation, suggesting that bacterial growth did not alter the pH value throughout the assay. However, the yellow halos surrounding the LF-loaded disks indicate that LF diffusion into the agar acidified the media.

To obtain insight into pH-responsive antibacterial activity, the BE-PVA/LF mats were further examined at pH 5.4, 7.4, and 8.4 using a suspension method against *S. aureus* ATCC 29213 and *E. coli* ATCC 25922.[73] MRSA was not examined in this experiment because it exhibited comparable responses to *S. aureus* when using the disk diffusion method. The LF loading levels in the mats were set to 0.005%, based on MIC values for *S. aureus* and *E. coli* (Table S2, ESI†). No growth was observed for mats containing large amounts of LF (*i.e.* 10, 20, or 25 LF wt%). BE-PVA mats (with no LF) were included, along with no mats (*e.g.* bacteria alone) as controls.

Fig. 9 shows the population of bacteria expressed in log(CFU per mL) as a measure of antibacterial activity. For *E. coli*, the cell density increased from 10^6 to 10^8 CFU per mL over 72 h at all tested pH values when it was incubated alone (*e.g.* no mats) (Fig. 9a). In the presence of BE-PVA mats, the bacteria concentration increased to 10^7 CFU per mL, suggesting that the bacterial growth appears to be inhibited to some degree, regardless of the pH (Fig. 9b). When incubated with BE-PVA/LF mats, the growth of *E. coli* was noticeably inhibited. Furthermore, such inhibition was observed to be pH-dependent as the growth decreased to zero at both pH 8.4 and pH 7.4, while it decreased to 10^4 at the acidic pH of 5.4 (Fig. 9c). This result is consistent with pH-responsive antibacterial activities determined by the disk-diffusion method. Furthermore, the trend is well aligned with pH-responsive degradation and the LF release profile in our earlier studies, indicating that the greater antibacterial activity of BE-PVA/LF mats at pH = 8.4 is attributed to their pH-responsive release of encapsulated LF upon degradation through the cleavage of BE bonds.

For *S. aureus*, similar results were observed for the controls, *i.e.* growth with no mats and slight inhibition of growth with BE-PVA mats (Fig. 9d and e). However, when incubated with BE-PVA/LF mats, the cell density decreased to 10^4–10^2 CFU per mL depending on the pH in 48 h and then increased to 10^5–10^6 CFU per mL (Fig. 9f). This result suggests that the amount of LF released from BE-PVA/LF mats was insufficient to eradicate *S. aureus* entirely, leading to either a comeback over-time or the emergence of resistant cells. Despite this, the observed growth reduction was pH-dependent.

Hemocompatibility and cytocompatibility of BE-PVA/LF mats

Since wound dressings are required to come into direct contact with wounds and consequently blood, the hemocompatibility of BE-PVA nanofiber mats with and without LF (0.005% loading level) was assessed with Sprague Dawley rat RBCs. An i*n vitro* hemolysis assay was used to follow the amount of hemoglobin to determine the %hemolysis of the tested mats. As seen in Fig. S19 (ESI†), the %hemolysis was 1.3% ± 0.3% for BE-PVA/LF (0.005%) and 1.2 ± 0.3 for LF-free BE-PVA mats suggesting that both mats are non-hemolytic. This implies that BE/PVA nanofibrous mats support an appropriate wound-healing environment without compromising blood components.

Furthermore, the biocompatibility of the mats was tested with human foreskin fibroblast HFF-1, along with human

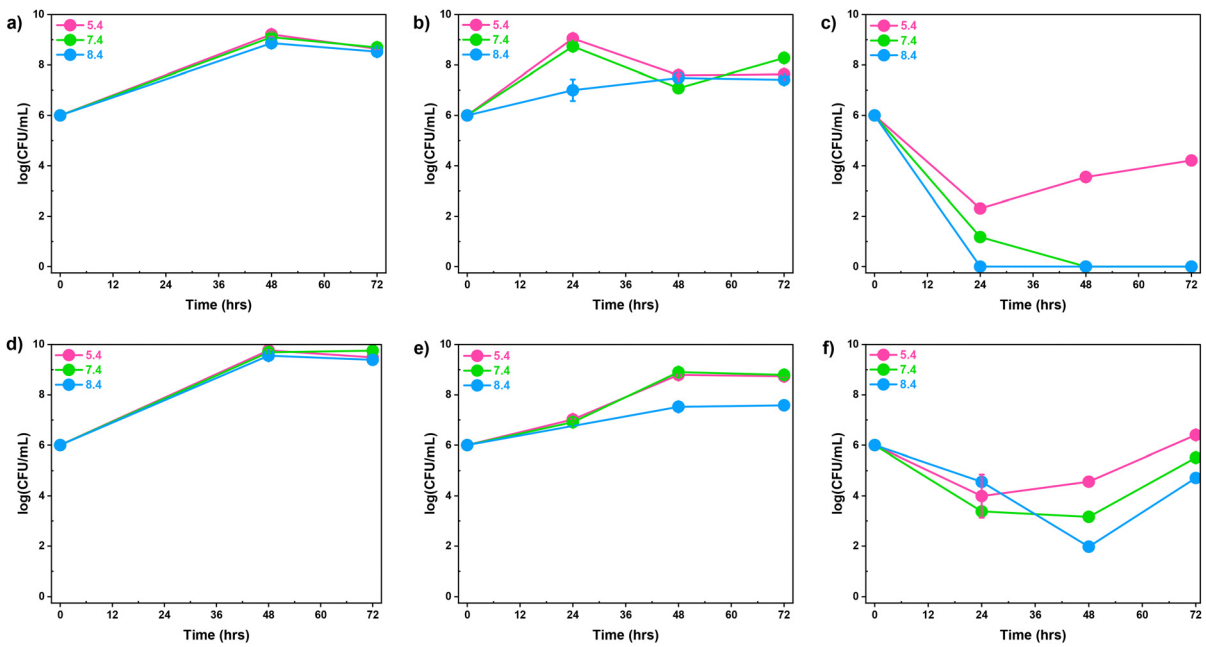

Fig. 9 Growth of *E. coli* ATCC 25922 (a)–(c) and *S. aureus* ATCC 29213 (d)–(f) incubated with no mats (*e.g.* bacteria alone) (a) and (b), BE-PVA mats (b) and (e), and BE-PVA/LF (0.005 wt%) at pH = 5.4, 7.4, and 8.4 over 72 h, determined by the suspension method.

embryonic kidney HEK293 cells. They were incubated with BE-PVA with and without LF (0.005%) for 72 h. As seen in Fig. S20 (ESI†), the BE-PVA/LF mats had the %viability of both cells to be >95% after 24 h incubation and >82% after 72 h incubation. Similar cell viabilities were observed for unloaded BE-PVA mats, which could be attributed to the loading level of LF being too low to be differentiated for viability. These results suggest that the BE-PVA/LF mats are biocompatible with healthy epidermal cells and thus skin tissues.

Given our promising results *in vitro* demonstrating good hemocompatibility, cytocompatibility, and antibacterial activities, the developed BE-PVA nanofibers could be evaluated *in vivo* (animal model) (as tested for hydrogels)[74,75] to further investigate their feasibility toward smart wound dressings.

Conclusion

In this work we studied the use of BE chemistry for the development of effective e-spun PVA nanofibers crosslinked with degradable BE bonds to promote wound healing. The newly synthesized phenyldiboronic acid with ethylene spacer (DBA-E) was revealed to be non-toxic to cells up to 9 μM and have a lower pK_a value of 7.7 and thus proved to be an effective crosslinker for e-spun PVA nanofibers crosslinked through the formation of BE bonds, confirmed by ^{11}B NMR and FT-IR spectroscopies as well as microscopic analysis. The amount of DBA-E as the BA/2OH mole equivalent ratio significantly influenced the extent of crosslinking as gel content and thermal properties of the fabricated BA-PVA nanofibers. These nanofibers degraded in response to multiple stimuli such as pH, H_2O_2, and glucose. Such a stimuli-responsive degradation could be attributed to the cleavage of BE bonds under acidic and alkaline pH conditions as well as in the presence of H_2O_2, while their transesterification with Glu, confirmed by ^{1}H NMR analysis with a newly synthesized small molecule pinacol-conjugated DBA (DBA-EP). Furthermore, the degradation of the nanofibers appeared to be faster at pH 8.4, in the presence of 1 mM hydrogen peroxide, and Glu at 126 mg dL^{-1} with NaOH, compared with their counterparts. This trend was consistent with the release profile of encapsulated LF from the fibers, suggesting that LF release is greatly attributed to their stimuli-responsive degradation. LF-loaded BE-PVA fibrous mats exhibit antibacterial activity against both Gram-positive and Gram-negative bacteria, particularly more effective against *E. coli* at a typical wound pH of 8.4. These results, combined with non-hemolysis and non-cytotoxicity, demonstrate that the developed BE-crosslinked e-spun PVA fibers have great potential as highly valued materials for wound dressing and healing.

Data availability

The data collected throughout the course of the study are presented and detailed within the main sections of the manuscript and the ESI.†

Conflicts of interest

There are no conflicts to declare.

Acknowledgements

This work is supported by the Natural Science and Engineering Research Council (NSERC) in Canada through the Discovery Grant, Collaborative Research and Training Experience Training (CREATE) Program entitled Polymer Nanoparticles Drug Delivery (PoND), and a Canada Research Chair (CRC) Award. PS is supported by a Lallemand Graduate Studentship. JKO was entitled to Tier II CRC in Nanobioscience (2011–2021). The authors acknowledge Dr Nooshin Movahed at the Center for NanoScience Research (CeNSR) for the SEM measurements, Dr Heng Jian from the Centre for Biological Applications of Mass Spectrometry (CBAMS) for help with the mass-spectrometry experiments, and Dr Kirill Levin from McGill University's MC2 Facility for help with the solid-state NMR measurements.

References

1 L. Shang, Y. Yu, Y. Liu, Z. Chen, T. Kong and Y. Zhao, *ACS Nano*, 2019, **13**, 2749–2772.
2 A. Greiner and J. H. Wendorff, *Angew. Chem., Int. Ed.*, 2007, 46, 5670–5703.
3 S. Agarwal, A. Greiner and J. H. Wendorff, *Prog. Polym. Sci.*, 2013, **38**, 963–991.
4 J. Xue, T. Wu, Y. Dai and Y. Xia, *Chem. Rev.*, 2019, **119**, 5298–5415.
5 Z. Chen, Z. Chen, A. Zhang, J. Hu, X. Wang and Z. Yang, *Biomater. Sci.*, 2016, **4**, 922–932.
6 S. Jiang, Y. Chen, G. Duan, C. Mei, A. Greiner and S. Agarwal, *Polym. Chem.*, 2018, **9**, 2685–2720.
7 C. Cleeton, A. Keirouz, X. Chen and N. Radacsi, *ACS Biomater. Sci. Eng.*, 2019, **5**, 4183–4205.
8 A. Alam, R. Karmakar, A. K. Rengan and M. Khandelwal, *ACS Biomater. Sci. Eng.*, 2023, **9**, 3160–3184.
9 Y. Dong, S. Fu, J. Yu, X. Li and B. Ding, *Adv. Funct. Mater.*, 2024, **34**, 2311199.
10 M. Abrigo, S. L. McArthur and P. Kingshott, *Macromol. Biosci.*, 2014, **14**, 772–792.
11 A. Memic, T. Abudula, H. S. Mohammed, K. Joshi Navare, T. Colombani and S. A. Bencherif, *ACS Appl. Bio Mater.*, 2019, **2**, 952–969.
12 R. S. Ambekar and B. Kandasubramanian, *Eur. Polym. J.*, 2019, **117**, 304–336.
13 S. Parham, A. Z. Kharazi, H. R. Bakhsheshi-Rad, M. Kharaziha, A. F. Ismail, S. Sharif, M. Razzaghi, S. Rama-Krishna and F. Berto, *Adv. Eng. Mater.*, 2022, **24**, 2101460.
14 L. Yao, T. W. Haas, A. Guiseppi-Elie, G. L. Bowlin, D. G. Simpson and G. E. Wnek, *Chem. Mater.*, 2003, **15**, 1860–1864.
15 M. Wang, J. Bai, K. Shao, W. Tang, X. Zhao, D. Lin, S. Huang, C. Chen, Z. Ding, J. Ye and C. Vasile, *Int. J. Polym. Sci.*, 2021, **2021**, 1–16.

16 N. Ben Halima, *RSC Adv.*, 2016, **6**, 39823–39832.
17 B. Bolto, T. Tran, M. Hoang and Z. Xie, *Prog. Polym. Sci.*, 2009, **34**, 969–981.
18 W. H. Han, Q. Y. Wang, Y. Y. Kang, L. R. Shi, Y. Long, X. Zhou and C. C. Hao, *Nanoscale*, 2023, **15**, 15513–15551.
19 B. Golba, O. I. Kalaoglu-Altan, R. Sanyal and A. Sanyal, *ACS Appl. Polym. Mater.*, 2021, **4**, 1–17.
20 R. Merckx, V. Dhaware, M. N. Leiske, K. De Clerck and R. Hoogenboom, *Chem. Mater.*, 2024, **36**, 9189–9206.
21 D. Nataraj, R. Reddy and N. Reddy, *Eur. Polym. J.*, 2020, **124**, 109484.
22 L. Gautam, S. G. Warkar, S. I. Ahmad, R. Kant and M. Jain, *Polym. Eng. Sci.*, 2022, **62**, 225–246.
23 K. C. de Castro, E. K. Silva, M. G. N. Campos and L. H. I. Mei, *ACS Appl. Nano Mater.*, 2022, **5**, 12616–12625.
24 J. Y. Wu, C. W. Ooi, C. P. Song, C. Y. Wang, B. L. Liu, G. Y. Lin, C. Y. Chiu and Y. K. Chang, *Carbohydr. Polym.*, 2021, **262**, 117910.
25 A. G. Destaye, C. K. Lin and C. K. Lee, *ACS Appl. Mater. Interfaces*, 2013, **5**, 4745–4752.
26 H. Y. Huang, A. Skripka, L. Zaroubi, B. L. Findlay, F. Vetrone, C. Skinner, J. K. Oh and L. A. Cuccia, *ACS Appl. Bio Mater.*, 2020, **3**, 7219–7227.
27 Y. Li and S. Yao, *Polym. Degrad. Stab.*, 2017, **137**, 229–237.
28 G. Mugnaini, R. Gelli, L. Mori and M. Bonini, *ACS Appl. Polym. Mater.*, 2023, **5**, 9192–9202.
29 G. M. Scheutz, J. J. Lessard, M. B. Sims and B. S. Sumerlin, *J. Am. Chem. Soc.*, 2019, **141**, 16181–16196.
30 D. B. Tiz, F. A. Vicente, A. Kroflič and B. Likozar, *ACS Sustainable Chem. Eng.*, 2023, **11**, 13836–13867.
31 R. M. LoPachin and T. Gavin, *Chem. Res. Toxicol.*, 2014, **27**, 1081–1091.
32 M. Chen, Y. F. Li and F. Besenbacher, *Adv. Healthcare Mater.*, 2014, **3**, 1721–1732.
33 C. Huang, S. J. Soenen, J. Rejman, B. Lucas, K. Braeckmans, J. Demeester and S. C. De Smedt, *Chem. Soc. Rev.*, 2011, **40**, 2417–2434.
34 K. Chen, Y. Li, Y. Li, Y. Tan, Y. Liu, W. Pan and G. Tan, *J. Nanobiotechnol.*, 2023, **21**, 237.
35 W. L. A. Brooks and B. S. Sumerlin, *Chem. Rev.*, 2016, **116**, 1375–1397.
36 S. Chatterjee, E. V. Anslyn and A. Bandyopadhyay, *Chem. Sci.*, 2021, **12**, 1585–1599.
37 S. Cho, S. Y. Hwang, D. X. Oh and J. Park, *J. Mater. Chem. A*, 2021, **9**, 14630–14655.
38 X. Zhang, Y. Zhao, S. Wang and X. Jing, *Mater. Chem. Front.*, 2021, **5**, 5534–5548.
39 A. Stubelius, S. Lee and A. Almutairi, *Acc. Chem. Res.*, 2019, **52**, 3108–3119.
40 R. Pan, G. Liu, Y. Zeng, X. He, Z. Ma, Y. Wei, S. Chen, L. Yang and L. Tao, *Polym. Chem.*, 2021, **12**, 2457–2463.
41 G. T. Williams, A. C. Sedgwick, S. Sen, L. Gwynne, J. E. Gardiner, J. T. Brewster, 2nd, J. R. Hiscock, T. D. James, A. T. A. Jenkins and J. L. Sessler, *Chem. Commun.*, 2020, **56**, 5516–5519.
42 A. Ali, S. Saroj, S. Saha, T. Rakshit and S. Pal, *ACS Appl. Bio Mater.*, 2023, **6**, 745–753.
43 K. Sato, S. Shimizu, K. Awaji, O. Hitomi and J. I. Anzai, *J. Colloid Interface Sci.*, 2018, **510**, 302–307.
44 W. Shi, B. Hass, M. A. Kuss, H. Zhang, S. Ryu, D. Zhang, T. Li, Y. L. Li and B. Duan, *Carbohydr. Polym.*, 2020, **233**, 115803.
45 Y. Guan and Y. Zhang, *Chem. Soc. Rev.*, 2013, **42**, 8106–8121.
46 L. Terriac, J. J. Helesbeux, Y. Maugars, J. Guicheux, M. W. Tibbitt and V. Delplace, *Chem. Mater.*, 2024, **36**, 6674–6695.
47 B. Liu, Y. Kong, O. A. Alimi, M. A. Kuss, H. Tu, W. Hu, A. Rafay, K. Vikas, W. Shi, M. Lerner, W. L. Berry, Y. Li, M. A. Carlson and B. Duan, *ACS Nano*, 2023, **17**, 3847–3864.
48 M. H. Othman, Y. Ito and J. Akimoto, *ACS Appl. Polym. Mater.*, 2022, **4**, 5047–5055.
49 R. Guo, Q. Su, J. Zhang, A. Dong, C. Lin and J. Zhang, *Biomacromolecules*, 2017, **18**, 1356–1364.
50 S. N. Casillas-Popova, N. D. Lokuge, B. Andrade-Gagnon, F. R. Chowdhury, C. D. Skinner, B. L. Findlay and J. K. Oh, *Macromol. Biosci.*, 2024, **24**, e2400217.
51 W. L. A. Brooks, C. C. Deng and B. S. Sumerlin, *ACS Omega*, 2018, **3**, 17863–17870.
52 S. Soundararajan, M. Badawi, C. M. Kohlrust and J. H. Hagernan, *Anal. Biochem.*, 1989, **178**, 125–134.
53 S. N. Casillas-Popova, N. D. Lokuge, B. Andrade-Gagnon, F. R. Chowdhury, C. D. Skinner, B. L. Findlay and J. K. Oh, *Macromol. Biosci.*, 2024, **24**, e2400217.
54 L. B. Reller, M. Weinstein, J. H. Jorgensen and M. J. Ferraro, *J. Clin. Infect. Dis.*, 2009, **49**, 1749–1755.
55 T. K. Mukherjee, in *Practical approach to mammalian cell and organ culture*, Springer, 2023, pp. 527–587.
56 T. L. Riss, R. A. Moravec, A. L. Niles, S. Duellman, H. A. Benink, T. J. Worzella and L. Minor, *Assay guidance manual*, 2016.
57 D. Zarzeczańska, A. Adamczyk-Woźniak, A. Kulpa, T. Ossowski and A. Sporzyński, *Eur. J. Inorg. Chem.*, 2017, 4493–4498.
58 A. Kilic, E. Aytar and L. Beyazsakal, *Energy Technol.*, 2021, **9**, 2100478.
59 T. Patranika, K. Märker, S. Paul, A. J. Naylor, J. Mindemark, K. Edström and G. Hernández, *ACS Appl. Polym. Mater.*, 2024, **6**, 12429–12440.
60 J. W. E. Weisse and D. Bryce, *J. Phys. Chem. A*, 2010, **114**, 5119–5131.
61 E. L. Daniels, J. R. Runge, M. Oshinowo, H. S. Leese and A. Buchard, *ACS Appl. Energy Mater.*, 2023, **6**, 2924–2935.
62 R. Nishiyabu, Y. Takahashi, T. Yabuki, S. Gommori, Y. Yamamoto, H. Kitagishi and Y. Kubo, *RSC Adv.*, 2019, **10**, 86–94.
63 M. Mukai, W. Ma, K. Ideta and A. Takahara, *Polymer*, 2019, **178**, 121581.
64 X. P. Zhang, B. B. Wang, W. X. Li, W. M. Fei, Y. Cui and X. D. Guo, *Eur. J. Pharm. Biopharm.*, 2021, **160**, 1–8.
65 D. A. Ossipov, S. Piskounova and J. Hilborn, *Macromolecules*, 2008, **41**, 3971–3982.
66 N. Tiwari, E. R. Osorio-Blanco, A. Sonzogni, D. Esporrin-Ubieto, H. Wang and M. Calderon, *Angew. Chem., Int. Ed.*, 2022, **61**, e202107960.

67 P. Yang, Z. Zhu, T. Zhang, W. Zhang, W. Chen, Y. Cao, M. Chen and X. Zhou, *Small*, 2019, **15**, e1902823.
68 L. A. Schneider, A. Korber, S. Grabbe and J. Dissemond, *Arch. Dermatol. Res.*, 2007, **298**, 413–420.
69 J. Hudzicki, *Am. Soc. Microbiol.*, 2009, **15**, 1–23.
70 *Clinical and Laboratory Standards Institute, Performance standards for antimicrobial susceptibility testing (M100, 35th ed.), Report M100*, USA, 2025.
71 K. E. Morton and S. H. Coghill, *Antibiotics*, 2024, **13**, 594.
72 F. Sandru, E. Poenaru, S. Stoleru, A. M. Radu, A. M. Roman, C. Ionescu, A. Zugravu, J. M. Nader and L. C. Baicoianu-Nitescu, *Antibiotics*, 2025, **14**, 53.
73 A. Amarjargal, O. Cegielska, D. Kolbuk, B. Kalaska and P. Sajkiewicz, *ACS Appl. Mater. Interfaces*, 2023, **16**, 153–165.
74 M. Liu, R. Ding, Z. Li, N. Xu, Y. Gong, Y. Huang, J. Jia, H. Du, Y. Yu and G. Luo, *Adv. Sci.*, 2024, **11**, e2306602.
75 D. Rybak, J. Du, P. Nakielski, C. Rinoldi, A. Kosik-Koziol, A. Zakrzewska, H. Wu, J. Li, X. Li, Y. Yu, B. Ding and F. Pierini, *Adv. Healthcare Mater.*, 2025, **14**, e2404274.